arXiv:physics/0511244v1 [physics.optics] 29 Nov 2005

Tuning quadratic nonlinear photonic crystal fibers for zero group-velocity mismatch

Morten Bache, Hanne Nielsen, Jesper Lægsgaard, and Ole Bang

COM•DTU, Technical University of Denmark, Bld. 345v, DK-2800 Lyngby, Denmark

Compiled February 2, 2008

We consider an index-guiding silica photonic crystal fiber with a triangular air-hole structure and a poled quadratic nonlinearity. By tuning the pitch and the relative hole size, second-harmonic generation with zero group-velocity mismatch is found for any fundamental wavelength above 780 nm. The phase-velocity mismatch has a lower limit with coherence lengths in the micron range. The dimensionless nonlinear parameter is inversely proportional to the pitch and proportional to the relative hole size. Selected cases show bandwidths suitable for 20 fs pulse-conversion with conversion efficiencies as high as 25%/mW. © 2008 Optical Society of America

OCIS codes: 060.2280, 060.2400, 060.4370, 320.7110

Relying on quadratic nonlinearities, second-harmonic generation (SHG) is widely used for efficient wavelength conversion devices in order to extend the spectral range of laser sources and to do all-optical wavelength multiplexing. Efficient conversion from the the fundamental to the second-harmonic (SH) mode requires a small phase mismatch between them. Phase matching to the lowest order is typically achieved through a quasi-phase matching (QPM) technique,[1] whereby the group-velocity mismatch (GVM) sets the limits to device length and bandwidth for pulsed SHG. In conventional fibers, SHG with near-zero GVM was found for restricted wavelengths,[2] while zero GVM was predicted using mode-matching.[3] For bulk media zero GVM was found for restricted wavelengths by spectrally noncritical phase matching,[4] and by combining non-collinear QPM with a pulse-front tilt.[5]

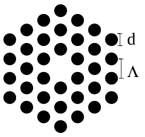

Fig. 1. Sketch of a triangular structured index-guiding PCF with pitch Λ and air-hole diameter d.

Here we investigate efficient pulsed SHG in a poled silica photonic crystal fiber (PCF), having a standard index-guiding triangular design with a single rod defect in the center (see Fig. 1). The main design parameters of the PCF are the pitch Λ and the relative hole size $D = d/\Lambda$. The nonlinearity is induced, *e.g.*, by thermal poling as has recently been demonstrated in PCFs.[6]

When the fundamental is assumed undepleted and continuous wave, the SHG efficiency is[2] $\eta \propto P_1 d_{\rm eff}^2 l_{\rm F}^2 {\rm sinc}^2(\Delta\beta l_{\rm F}/2)/A_{\rm ovl}$. The contributions to η of nonlinear nature are the fundamental power P_1, the nonlinear coefficient $d_{\rm eff}$ and the effective mode overlap area $A_{\rm ovl}$. Efficient SHG therefore requires a strong mode confinement within a small core and a small effective mode overlap area, as well as a strong nonlinear material response. The linear contributions to η are the fiber length $l_{\rm F}$ and the phase mismatch $\Delta\beta = 2\beta_1 - \beta_2$ between the modes (β_j are the mode propagation constants). The coherence length of the phase mismatch to the lowest order gives the range over which power is exchanged efficiently to the SH, but a QPM method can compensate for this. The SHG bandwidth is determined by the width of ${\rm sinc}^2(\Delta\beta l_{\rm F}/2)$, and since ultra-short pulses have broad spectra, efficient conversion requires a large bandwidth (small $\Delta\beta l_{\rm F}$). Reducing $l_{\rm F}$ does the trick, but this gives a poor efficiency. The first order contribution to $\Delta\beta$ is GVM, giving a temporal walk-off length l_W between the modes, so we must take $l_{\rm F} \leq l_W$. When GVM is zero, $l_W \to \infty$, and 2. order dispersion takes over, giving a larger bandwidth in a longer device.

In this Letter, we tune the phase-matching properties of SHG by exploiting the flexibility that PCFs offer in designing the dispersion properties.[7] Previous investigations[8] of SHG in PCFs considered the scalar case and found large bandwidths and strong modal overlaps for selected parameter values. Instead, we perform a detailed vectorial analysis over a continuous parameter space, and show zero GVM for any fundamental wavelength $\lambda_1 > 780$ nm by merely adjusting the pitch and the relative hole size. This is a much simpler way of removing GVM compared to previous methods,[3–5] and promises very large bandwidths due to its flexibility. The nonlinear properties of the SHG fiber design are also discussed.

We first focus on the linear dispersion. A fiber mode can be described by an effective index $n = c/v_{\rm ph}$, *i.e.*, the ratio of the speed of light c to the phase velocity of the mode $v_{\rm ph} = \omega/\beta$. The dispersive character of β gives a phase-velocity mismatch between the modes with frequencies ω_1 (fundamental) and $\omega_2 = 2\omega_1$ (SH), which we classify through the *index mismatch* $\Delta n = c[1/v_{\rm ph}(\omega_1) - 1/v_{\rm ph}(\omega_2)] = c[\beta_1/\omega_1 - \beta_2/\omega_2]$. For SHG the index mismatch is related to the lowest order phase mismatch as $\Delta\beta = 4\pi\Delta n/\lambda_1$. The mode group velocity is instead defined as $1/v_{\rm g} = \partial_\omega\beta$, $\partial_\omega \equiv \frac{\partial}{\partial\omega}$, giving a GVM (walk-off) parameter $d_{12} = [1/v_{\rm g}(\omega_1) - 1/v_{\rm g}(\omega_2)]$.

We calculated the dispersion with the MIT Photonic-

Bands (MPB) package.[9] Each unit cell contained $n_{\rm C}^2 = 32^2$ grid points, and the super cell contained $n_{\rm SC}^2 = 5^2$ unit cells. The fundamental mode frequency and group velocity were first calculated, followed by iterative calculations of the SH until $|\omega_2 - 2\omega_1| < 10^{-8}$. Subsequently, a perturbative approach[10] was used to introduce chromatic dispersion, allowing us to calculate data once over a large (D, β_1) parameter space for Λ unity, and perturbatively calculate the changes as Λ was varied.

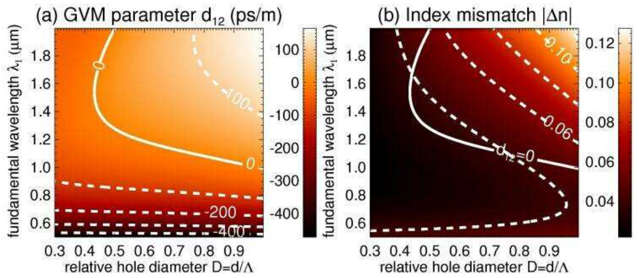

Fig. 2. Color maps of (a) d_{12} and (b) $|\Delta n|$ as function of D and λ_1, keeping the pitch $\Lambda = 1.6$ μm fixed. The solid contour in (a) shows $d_{12} = 0$ and it is repeated in (b).

Figure 2 shows the GVM and index mismatch in the (D, λ_1) parameter space, keeping the pitch fixed at $\Lambda = 1.6$ μm. Along the the solid contour $d_{12} = 0$: thus, zero GVM is possible for any $\lambda_1 > 1$ μm by choosing a proper D. Fig. 3(a) underlines that this is a general trend: there the zero-GVM contour is shown for selected pitches, and we found $d_{12} = 0$ can be achieved for any $\lambda_1 > 0.78$ μm. Note that in Fig. 2(b) $|\Delta n| > 0$, even with non-zero GVM, so the index mismatch cannot be zero. This holds also for other Λ values, so efficient SHG will require additional phase-matching such as QPM.

Figure 3(b) shows the values of the index mismatch as the zero-GVM contour is traversed. For $\Lambda = 0.70,\ 1.0$ and 1.6 μm a cusp appears around $\lambda_1 \simeq \Lambda$, after which $|\Delta n|$ increases with λ_1. This is because the fundamental mode is no longer well-confined in the core while the SH, having a smaller wavelength, is still well confined. Conversely, for the considered wavelengths the modes are always well confined for $\Lambda = 3.5,\ 5.0$ μm, explaining why a small $|\Delta n|$ is observed there. The coherence length $l_{\rm coh} = \pi/\Delta\beta = \lambda_1/(4\Delta n)$ is shown for completeness in Fig. 3(c), giving typical values in the micron range.

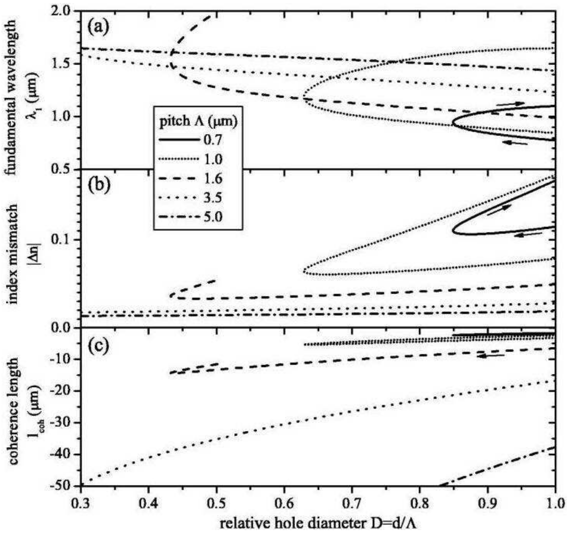

Fig. 3. Extracted zero GVM contours showing (a) λ_1, (b) $|\Delta n|$ and (c) $l_{\rm coh}$. The curves in (b)-(c) for $\Lambda = 1.6$ μm abruptly stop because $\lambda_1 \in [0.5, 2]$ μm. The arrows indicate the contour-direction for increasing λ_1.

Let us focus on the telecom, Nd:YAG and Ti:Sapphire operating wavelengths ($\lambda_1 = 1.55$ μm, 1.06 μm and 0.80 μm, respectively.) In Fig. 4(a) we then show the D-value required to get zero GVM as Λ is changed. For $\lambda_1 = 0.80$ μm zero GVM requires very large D-values, *e.g.*, $D = 0.96$ for $\Lambda = 0.70$. For such D-values deviations from the ideal circular holes must be expected, which might influence the results presented here. However, to our knowledge it is the first time that zero GVM has been demonstrated for SHG in any material for this wavelength. For $\lambda_1 = 1.06$ μm the lowest required D-values are in a range where the ideal round holes should be preserved. The curves stop for larger Λ because it is no longer possible to get $d_{12} = 0$ (it would require $D > 1$, which is unphysical.) For $\lambda_1 = 1.55$ μm a wide range of possibilities are offered, but it is advantageous to have $\Lambda < 2$ μm because D increases, which leads to higher intensities due to stronger mode confinement in a smaller core diameter $d_{\rm c} = \Lambda(2 - D)$. In Fig. 4 we calculate the SHG bandwidth $\Delta\lambda$ of the $\mathrm{sinc}^2(\Delta\beta l_{\rm F}/2)$ term by expanding[1,5] $\Delta\beta(\lambda_1 + \Delta\lambda) = \sum_m (m!)^{-1}\Delta\lambda^m \partial_\lambda^m \Delta\beta$, and assuming that a QPM grating compensates the $m = 0$ term (as is routinely done in conventional fibers[2]). Since $d_{12} = 0$, the 2. order dispersion dominates yielding very large bandwidths. Moreover, because $d_{12} = 0$ the bandwidth scales as $\Delta\lambda \propto l_{\rm F}^{-1/2}$ (instead of $\Delta\lambda \propto l_{\rm F}^{-1}$ for $d_{12} \neq 0$), and thus a longer device can be created without loosing too much bandwidth. Note also in Fig. 2(a) the turn of the zero-GVM contour around $D = 0.43$ and $\lambda_1 = 1.6$ μm, implying that the $m = 2$ term vanishes, giving an increasing bandwidth as observed in Fig. 4(b). It is still unclear to what extend the exact location of this turning point is influenced by parameter uncertainties.

Using the reductive perturbation method,[11] the dimensionless nonlinear equations for SHG are

$$(\partial_z - i\tilde{D}_1\partial_t^2)u_1 = i\sigma u_1^* u_2 e^{-i\Delta\beta z l_{\rm F}}, \qquad (1)$$

$$(\partial_z - \tilde{d}_{12}\partial_t - i\tilde{D}_2\partial_t^2)u_2 = i\sigma u_1^2/2 e^{i\Delta\beta z l_{\rm F}}, \qquad (2)$$

We have assumed a weak nonlinearity [so $\mathbf{E}_j(\mathbf{r}) = A_j(z,t)\mathbf{e}_j(\mathbf{x})e^{i(\beta_j z - \omega_j t)} + $c.c., where $\mathbf{x} = (x, y)$,] uniform over the silica part of the super cell, and weak transverse variations in the refractive index so $\nabla\times(\nabla\times\mathbf{E}) = -\nabla^2\mathbf{E}$. The "retarded" coordinate z [traveling with velocity $v_{\rm g}(\omega_1)$] is normalized to $l_{\rm F}$, t to the input pulse length τ, $\tilde{d}_{12} = d_{12}l_{\rm F}/\tau$ and $\tilde{D}_j = l_{\rm F}/(2\tau^2)\partial_\omega^2\beta_j$. We define $A_j = u_j(2\Lambda^2 l_{\rm F}/N_j n_j a_j c\tau)^{1/2}$ so $N_j(z) = \int dt|u_j(z,t)|^2$

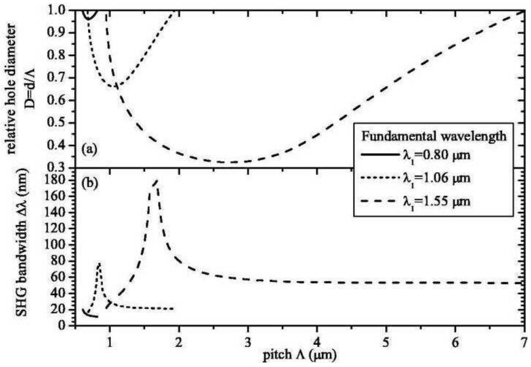

Fig. 4. Zero GVM contours vs. Λ with fixed λ_1s, showing (a) D as well as (b) $\Delta\lambda$ for a $l_{\mathrm{F}} = 10$ cm device.

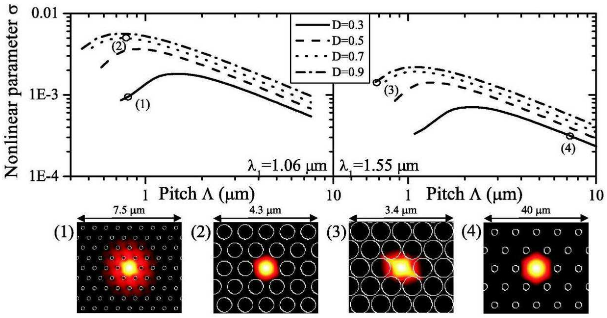

Fig. 5. Double-log plots of σ vs. Λ for $l_{\mathrm{F}} = 10$ cm and $\tau = 1$ ps. (1)-(4) show energy distributions of the FH modes from MPB. $n_{\mathrm{SC}} = 9$ to ensure localized modes.

is the photon number in the jth wave. The dimensionless nonlinear parameter is $\sigma = \rho l_{\mathrm{F}}(2\hbar\omega_1^2\omega_2/n_1^2 n_2 \varepsilon_0 c^3 \tau)^{1/2}$, where $\rho = (a_1^2 a_2)^{-1/2} |\int d\mathbf{x} \tilde{\mathbf{e}}_1^*(\mathbf{x}) \cdot \tilde{\chi}^{(2)}(\mathbf{x}) : \tilde{\mathbf{e}}_2(\mathbf{x}) \tilde{\mathbf{e}}_1^*(\mathbf{x})|$, $\tilde{\chi}^{(2)}(\mathbf{x})$ is the Fourier transform of the quadratic nonlinear dielectric tensor, $\tilde{\mathbf{e}}_j(\mathbf{x}) = \mathbf{e}_j(\mathbf{x})(\varepsilon_0 \Lambda^2 l_{\mathrm{F}}/\hbar\omega_j N_j)^{1/2}$ the dimensionless transverse modes from MPB and $a_j = \int d\mathbf{x} |\tilde{\mathbf{e}}_j(\mathbf{x})|^2$ the mode areas. Integrating over z in Eq. (2) gives $\eta = P_1 \rho^2 l_{\mathrm{F}}^2 \mathrm{sinc}^2(\Delta\beta l_{\mathrm{F}}/2) 2\omega_1^2/n_1^2 n_2 \varepsilon_0 c^3$. Thus, ρ^2 is the vectorial equivalent of $d_{\mathrm{eff}}^2/A_{\mathrm{ovl}}$ of Ref. 2.

The $\tilde{\chi}^{(2)}$ tensor is assumed to have the non-zero elements $\tilde{\chi}_{jji}^{(2)} = \tilde{\chi}_{jij}^{(2)} = \tilde{\chi}_{iij}^{(2)} = \tilde{\chi}_{iii}^{(2)}/3$, where i is the main direction of the poling voltage, and j is either of the 2 remaining directions.[12] The present problem has two degenerate solutions that are x- and y-polarized, respectively, so it will suffice to consider $i = x$. We used a realistic value $\tilde{\chi}_{xxx}^{(2)} = 1$ pm/V. The nonlinear parameter σ in Fig. 5 is calculated by fixing λ_1 and D (in contrast to Figs. 3,4, these curves are not zero-GVM contours.) As expected σ is seen to become larger as Λ is reduced as well as when D is increased, and we found the scaling $\sigma \propto D/\Lambda = d/\Lambda^2$. σ peaks when Λ takes values around the chosen fundamental wavelength λ_1, and drops for $\Lambda < \lambda_1$ because the fundamental mode has maximum core confinement at the peak [Fig. 5(2)], while it becomes more poorly confined when $\Lambda < \lambda_1$ [Fig. 5(1,3)]. Instead, the SH having $\lambda_2 = \lambda_1/2$ can stay confined longer as Λ is reduced, resulting in a poor modal overlap. [A similar effect gives the cusp in $|\Delta n|$ in Fig. 3(b).] For large D, a decent fundamental mode confinement is observed even for $\Lambda < \lambda_1$ [compare Fig. 5(3) with (1),] giving a shift in the peak towards smaller Λ. Finally, σ gets larger when λ_1 becomes smaller because if d and Λ are fixed, the light is better confined for smaller λ. Table 1 shows choices for efficient SHG with zero GVM using $\tau = 1$ ps and $l_{\mathrm{F}} = 10$ cm. The large bandwidths imply that pulses as short as $\tau_{\mathrm{lim}} = 21$ fs can be converted. The relative SHG efficiencies η/P_1 are as high as 25 %/mW.

To conclude, by tuning the pitch and relative hole size in a standard index-guiding silica PCF, we showed that SHG with zero GVM is possible for any $\lambda_1 > 780$ nm. This is a new and simple way to remove GVM, which in addition has conversion bandwidths suitable for down to 20 fs pulse-conversion. The SHG nonlinear parameter was inversely proportional to the pitch and proportional to the relative hole size, due to smaller mode overlap areas for lower pitches and larger relative hole sizes, and up to 25%/mW conversion efficiencies was found.

Support from The Danish Natural Science Research Council (FNU, grant no. 21-04-0506) is acknowledged. M. Bache's e-mail address is bache@com.dtu.dk.

References

1. M. M. Fejer, G. A. Magel, D. H. Jundt, and R. L. Byer, IEEE J. Quantum Electron. **28**, 2631 (1992).
2. P. G. Kazansky and V. Pruneri, J. Opt. Soc. Am. B **14**, 3170 (1997).
3. A. Arraf and C. M. de Sterke, IEEE J. Quantum Electron. **34**, 660 (1998).
4. N. E. Yu, J. H. Ro, M. Cha, S. Kurimura, and T. Taira, Opt. Lett. **47**, 1046 (2002).
5. S. Ashihara, T. Shimura, and K. Kuroda, J. Opt. Soc. Am. B **20**, 853 (2003).
6. D. Faccio, A. Busacca, W. Belardi, V. Pruneri, P. Kazansky, T. Monro, D. Richardson, B. Grappe, M. Cooper, and C. Pannell, Electron. Lett. **37**, 107 (2001).
7. A. Ferrando, E. Silvestre, J. Miret, and M. Andrés, Opt. Express **9**, 687 (2000).
8. T. M. Monro, V. Pruneri, N. G. R. Broderick, D. Faccio, P. G. Kazansky, and D. J. Richardson, IEEE Photon. Tech. Lett. **13**, 981 (2001).
9. S. Johnson and J. Joannopoulos, Opt. Express **8**, 173 (2001).
10. J. Lægsgaard, A. Bjarklev, and S. Libori, J. Opt. Soc. Am. B **20**, 443 (2003).
11. Y. Kodama and A. Hasegawa, IEEE J. Quant. Electr. **QE-23**, 510 (1987).
12. S. Kielich, IEEE J. Quant. Electr. **5**, 562 (1969).

Table 1. Selected parameters for SHG with zero GVM.

λ_1 μm	Λ μm	D	$\Delta\lambda$ nm	τ_{lim} fs	$\lvert l_{\mathrm{coh}} \rvert$ μm	σ 10^{-4}	η/P_1 $\frac{\%}{\mathrm{mW}}$
0.80	0.70	0.96	13	73	2.1	112	25
1.06	0.85	0.72	77	21	3.7	49.8	6.3
1.55	1.60	0.43	170	21	14.4	11.5	0.5